Geophysical Journal International

Geophys. J. Int. (2012) **189,** 6–18 doi: 10.1111/j.1365-246X.2012.05365.x

GJI Geodynamics and tectonics

New evidence for large earthquakes on the Central Iran plateau: palaeoseismology of the Anar fault

M. Foroutan,[1,2,3] M. Sébrier,[2,3] H. Nazari,[4] B. Meyer,[2,3] M. Fattahi,[5,6,7] A. Rashidi,[8] K. Le Dortz[2,3,*] and M. D. Bateman[6]

[1]*Geological Survey of Iran, Azadi Square, Meraj Avenue, PO Box* 13185–1494, *Tehran, Iran*
[2]*UPMC (Université Pierre et Marie Curie) Université Paris* 06, *ISTEP UMR* 7193, F-75005, *Paris, France. E-mail: mohammad.foroutan@upmc.fr*
[3]*CNRS, ISTEP, UMR* 7193, F-75005, *Paris, France*
[4]*Research Institute for Earth Sciences, Geological Survey of Iran, PO Box* 13185–1494, *Tehran, Iran*
[5]*The Institute of Geophysics, University of Tehran, Tehran, Iran*
[6]*Sheffield Centre for International Dryland Research, Department of Geography, University of Sheffield, Winter Street, Sheffield* S10 2TN, *UK*
[7]*The School of Geography, University of Oxford, OX1 3QY, UK*
[8]*Geological Survey of Iran, Postal Code* 7615736841, *Kerman, Iran*

Accepted 2012 January 5. Received 2011 November 24; in original form 2011 August 18

SUMMARY

The Central Iran plateau appears aseismic during the last few millenniums based on instrumental and historical seismic records. Nevertheless, it is sliced by several strike-slip faults that are hundreds of kilometres long. These faults display along-strike, horizontal offsets of intermittent gullies that suggest the occurrence of earthquakes in the Holocene. Establishing this is crucial for accurately assessing the regional seismic hazard. The first palaeoseismic study performed on the 200-km long, NS striking Anar fault shows that this right-lateral fault hosted three large ($M_w \approx 7$) earthquakes during the Holocene or possibly Uppermost Pleistocene for the older one. These three seismic events are recorded within a sedimentary succession, which is not older than 15 ka, suggesting an average recurrence of at most 5 ka. The six optically stimulated luminescence ages available provide additional constraints and allow estimating that the three earthquakes have occurred within the following time intervals: 4.4 ± 0.8, 6.8 ± 1 and 9.8 ± 2 ka. The preferred age of the more recent event, ranging between 3600 and 5200 yr, suggests that the fault is approaching the end of its seismic cycle and the city of Anar could be under the threat of a destructive earthquake in the near future. In addition, our results confirm a previous minimum slip rate estimate of 0.8 ± 0.1 mm yr^{-1} for the Anar fault indicating that the westernmost prominent right-lateral faults of the Central Iran plateau are characterized by slip rates close to 1 mm yr^{-1}. These faults, which have repeatedly produced destructive earthquakes with large magnitudes and long recurrence interval of several thousands of years during the Holocene, show that the Central Iran plateau does not behave totally as a rigid block and that its moderate internal deformation is nonetheless responsible for a significant seismic hazard.

Key words: Geomorphology; Continental tectonics: strike-slip and transform; Tectonics and landscape evolution; Palaeoseismology; Seismicity and tectonics.

INTRODUCTION

The Central Iran plateau is a wide region experiencing low GPS deformation rates and is commonly described as a rigid block (e.g. Jackson & McKenzie 1984; Vernant *et al.* 2004). The region (Fig. 1) is nonetheless sliced by several strike-slip faults with clear morphological traces (Walker & Jackson 2004; Meyer *et al.* 2006; Meyer & Le Dortz 2007) that contrast with the very few earthquakes recorded in the region (Ambraseys & Jackson 1998). Destructive earthquakes have occurred close to or along the Lut faulted borders only, and according to the historical and instrumental records (Ambraseys & Melville 1982; Ambraseys & Jackson 1998), the prominent right-lateral strike-slip faults inland remained quiescent for millenniums. Although the absence of historical record of earthquakes in remote and uninhabited desert does not mean an absence of earthquakes, knowledge of the behaviour of such faults and assessment of the regional seismic hazard requires palaeoseismic studies and depends on the selection of suitable trenching sites. This is the case for the region of the Dehshir and Anar faults. Although a recent

*Now at: Laboratoire de Géologie, ENS, UMR 8538, 75231 Paris, France.

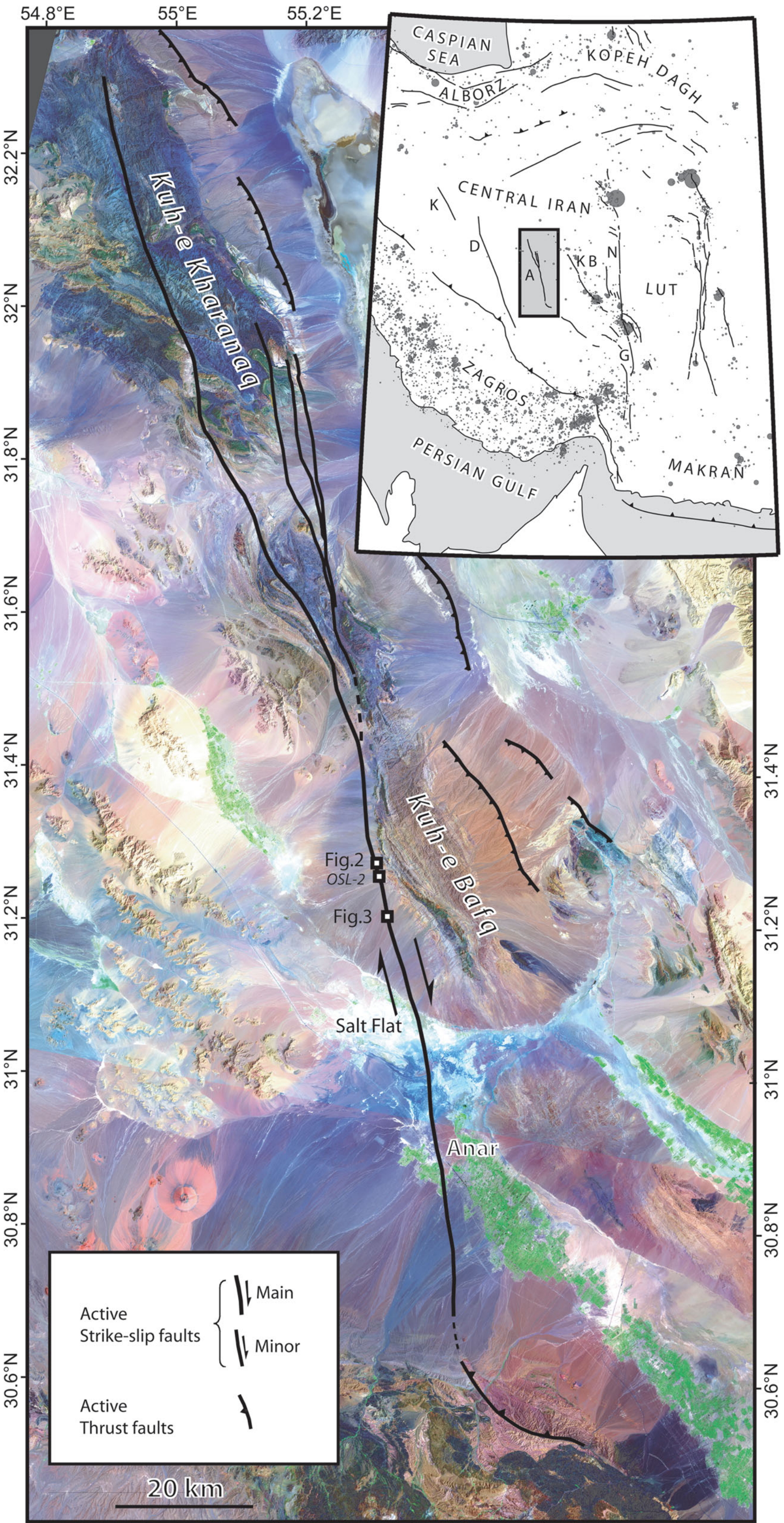

Figure 1. Landsat mosaic of the Anar fault area. White squares for location of photograph in Fig. 2, Quickbird extract in Fig. 3 and location of OSL-2 sampling site. Upper right-hand inset locates the area within a simplified seismotectonic map of Iran. K, D, A, KB, N and G, respectively for Kashan, Dehshir, Anar, Kuh Banan, Nayband and Gowk faults.

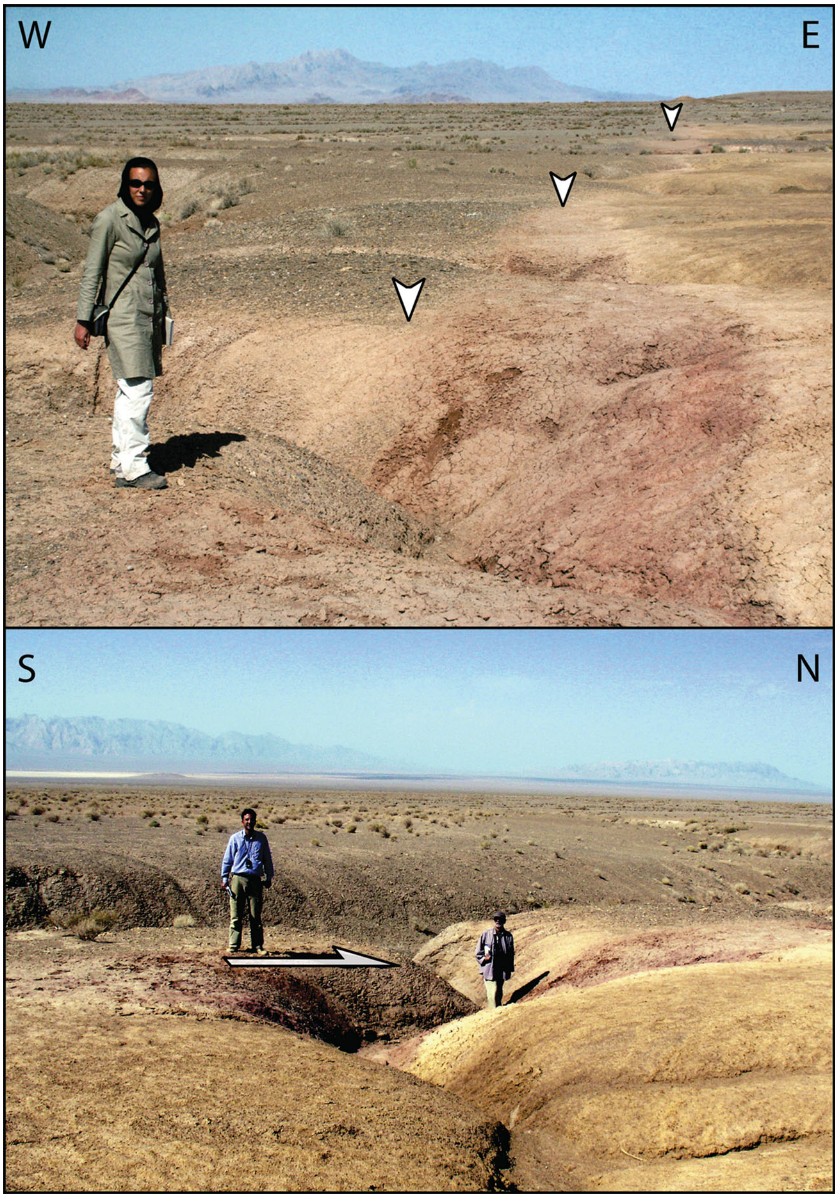

Figure 2. Field photograph of the Anar fault (vertical arrows, top panel) taken towards the north from 31.2764°N to 55.1304°E with emphasis on a 3-m right-lateral offset rill (horizontal arrow, bottom panel).

palaeoseismic study stated the occurrence of large and infrequent earthquakes on the Dehshir fault (Nazari *et al.* 2009; Fattahi *et al.* 2010), the seismic behaviour of the Anar fault is still to be assessed.

The Anar fault is a 200-km-long NS strike-slip fault located nearby 55°E, in the middle of the Central Iran plateau (Fig. 1). The northern part of the fault is located within a mountainous region where several closely spaced splays cut across the Kuh-e Kharanaq range. The southern portion of the fault runs along the Kuh-e Bafq range and cuts right across the western piedmont of the range and across the Anar salt flat. The fault goes through the populated city of Anar and further bends eastwards to reactivate a thrust fault to the south. According to ^{10}Be cosmic ray exposure (CRE) and optically stimulated luminescence (OSL) dating of cumulative offset of alluvial fans, the southern portion of the fault slips at a minimum rate of 0.8 mm yr^{-1} (Le Dortz *et al.* 2009). Both the sharpness of these cumulative offsets and the absence of along fault microseismicity suggest these offsets have accrued through large and infrequent earthquakes rather than by creeping. At a few places, the offset of small gullies that ranges between 2.5 and 3.5 m (Fig. 2) may be interpreted as the amount of coseismic slip during the last earthquake but clear evidence for a continuous and distinctive surface break is missing. Trenching appears therefore necessary to document earthquakes and access the recent seismic history of the fault.

SITE SELECTION AND TRENCH STRATIGRAPHY

We scrutinized the fault on Quickbird satellite imagery and in the field to select the most favourable place to conduct palaeoseismic investigations. The selected site is located 35 km north of the city of Anar along a very clear portion of the N175°E fault trace that is highlighted by an E-facing scarp (Fig. 3). This fault scarp is readily seen cutting across numerous rills and ephemeral streams that incise a fan surface characterized by a subdued bar-and-swale

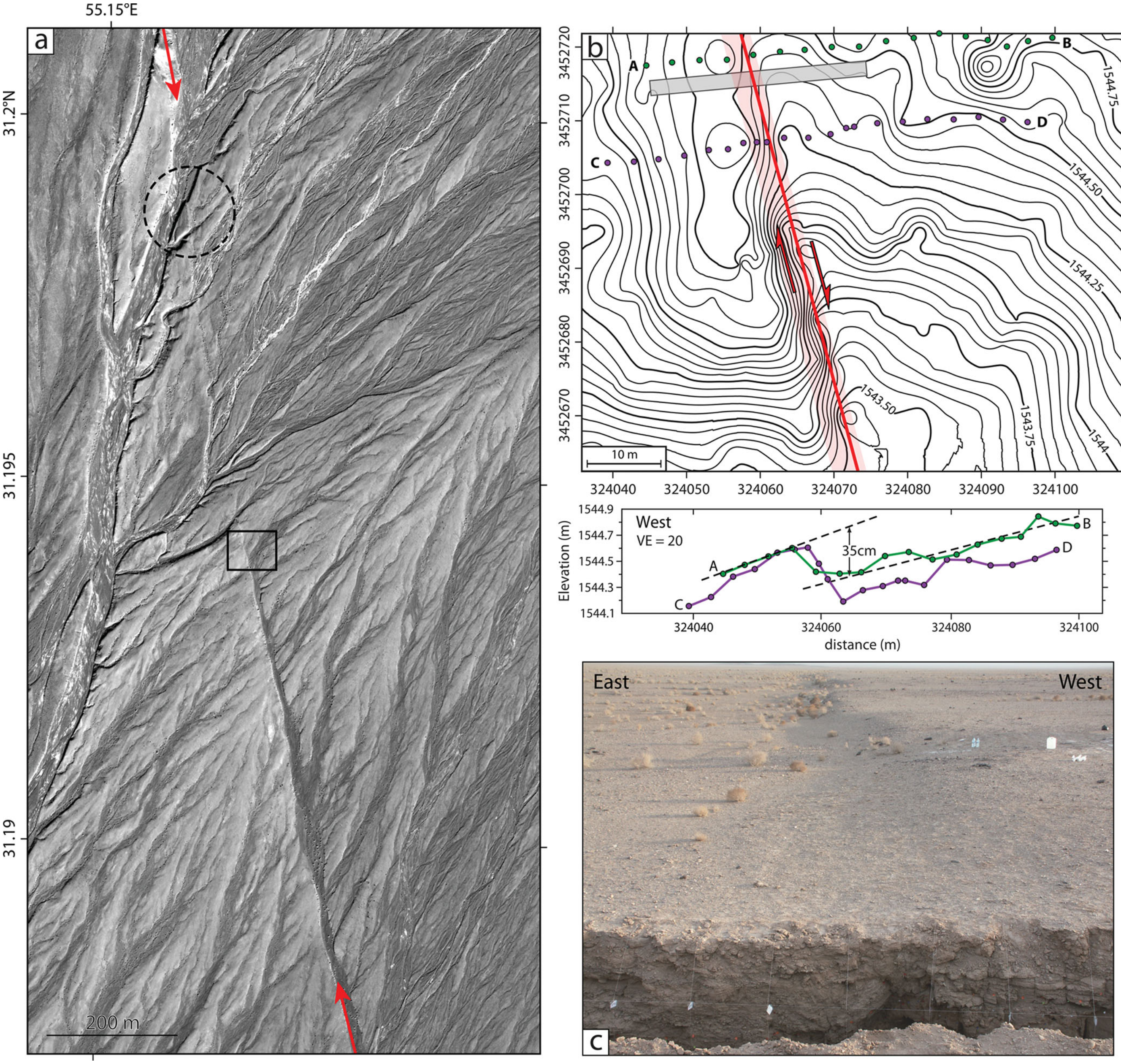

Figure 3. (a) Quickbird imagery of the Anar fault trace (red arrows) centred on the palaeoseismological site (rectangle). Circle indicates the 8 ± 0.5 m cumulative dextral-offset riser described as site 1 in Le Dortz *et al.* (2009). (b) Topographic DGPS map (top) and profiles (bottom) of the palaeoseismological site. Contour interval is 5 cm (survey data not tied to absolute elevation). The smooth and subdued E-facing fault scarp is indicated by a red overprint and the location of the trench by a rectangle. Violet and green dots locate the DGPS data points used for the topographic profiles. (c) Field photograph, looking south, of the E-facing fault scarp. The upper part of the southern trench wall is in the foreground. Three white labels that are 1-m spaced show scale on trench wall.

morphology. The abandoned alluvial fan surface comprises a loose desert pavement of varnished clasts separated by sandy–silty material. The smooth scarp has a minimum height of 35 cm near the excavation (Fig. 3b). South of the trench site, the scarp height increases progressively to reach 1 m where small streams, which have been dammed and channelled along the fault, rejuvenate this scarp. North of the trench site, the scarp height also increases, but the streams are wider and deeper than to the south and have been able to maintain their courses to flow across the fault trace. At the trench site, the possibility of damming small intermittent streams during the emplacement of the fan material is high and the possibility of subsequent erosion low, maximizing the chances to record the earthquakes coeval with alluvial aggradation and subsequent colluvial deposition. The next paragraphs report the observations gathered at the selected site, where trenching allowed us to distinguish three unambiguous events.

The eastern tip of the excavated trench is located about 5 km west of the Kuh-e Bafq range at 31.1953°N, 55.1536°E and 1544 m altitude above sea level (asl; Figs 1 and 3b). The trench strikes N85°E, it has a length of 28 m, a depth between 4.3 and 4.7 m and a width of some 1.5 m (Figs 3–5). Trench walls expose a total deposit thickness of 5.9 m with fairly flat, 0.1- to 1-m-thick beds that correspond to medium-distal, alluvial fan facies. Trench stratigraphy is relatively straightforward as these beds are continuous and easily correlated

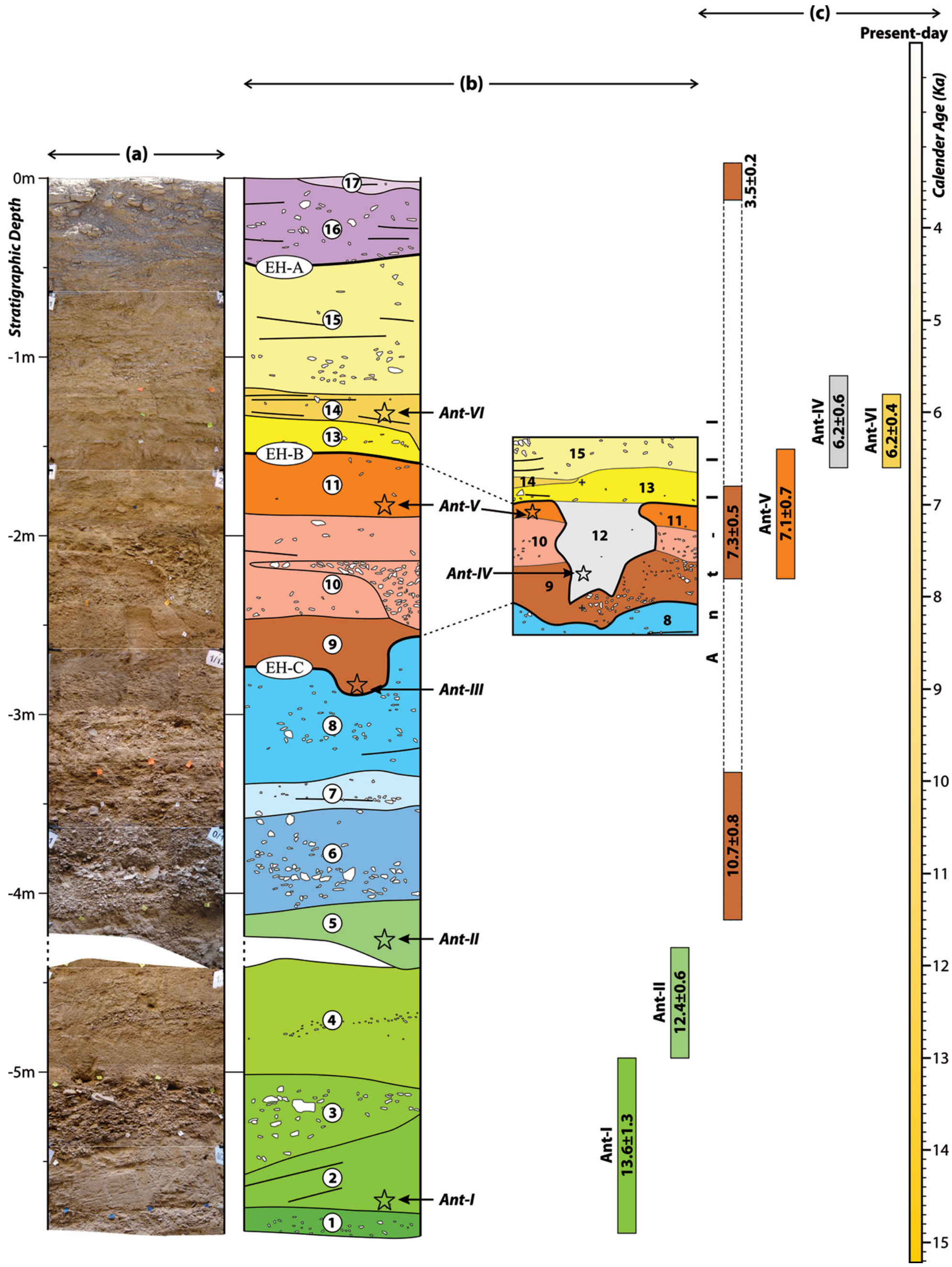

Figure 4. Composite photomosaic of the sediments exposed in the Anar trench excavation, (a) with top 4 m (between 11 and 12 m) east and bottom 2 m (between 19 and 20 m) west of the main fault zone, and (b) corresponding stratigraphic log of the units with vertical positions of dated samples. Numbers indicate units described in detail in Table 1. Three event horizons (EH-A, EH-B and EH-C) are shown as thick black lines (see text for discussion). (c) Stars locate the positions (see exact location in Fig. 5) of the six samples with OSL ages given.

across the fault zone located approximately in the middle of the trench (Fig. 5). Overall the beds found in the trench are composed of sands and gravels mixed with variable amounts of silt and clay, these deposits correspond mostly to a debris-flow dominated alluvial fan. Although debris flows and sheet floods appear to dominate, sediment dynamics is not easy to determine precisely for each bed due to the medium-distal deposit conditions.

A total of 17 units have been defined in the excavated trench (Table 1; Figs 4 and 5). The uppermost part of the trench, approximately the last metre, is made of the thinner units 13–17 containing smaller pebbles than the alluvial units 1–8 and an almost clay-free matrix contrary to the units 9–11. This last metre hence is made of run-off deposits. The only evidence for a significant break in alluvial sedimentation is the ≈0.15-m-thick, gypsiferous calcrete that is located towards the top of unit 11. This latter unit and units 9 and 10 correspond to reddish brown, mud-dominated debris flows. OSL was used to date the alluvial layers seen in the trench.

OSL DATING

Six lenses of fine sandy silts intercalated between fanglomerates at various depths below the surface were sampled for OSL in opaque

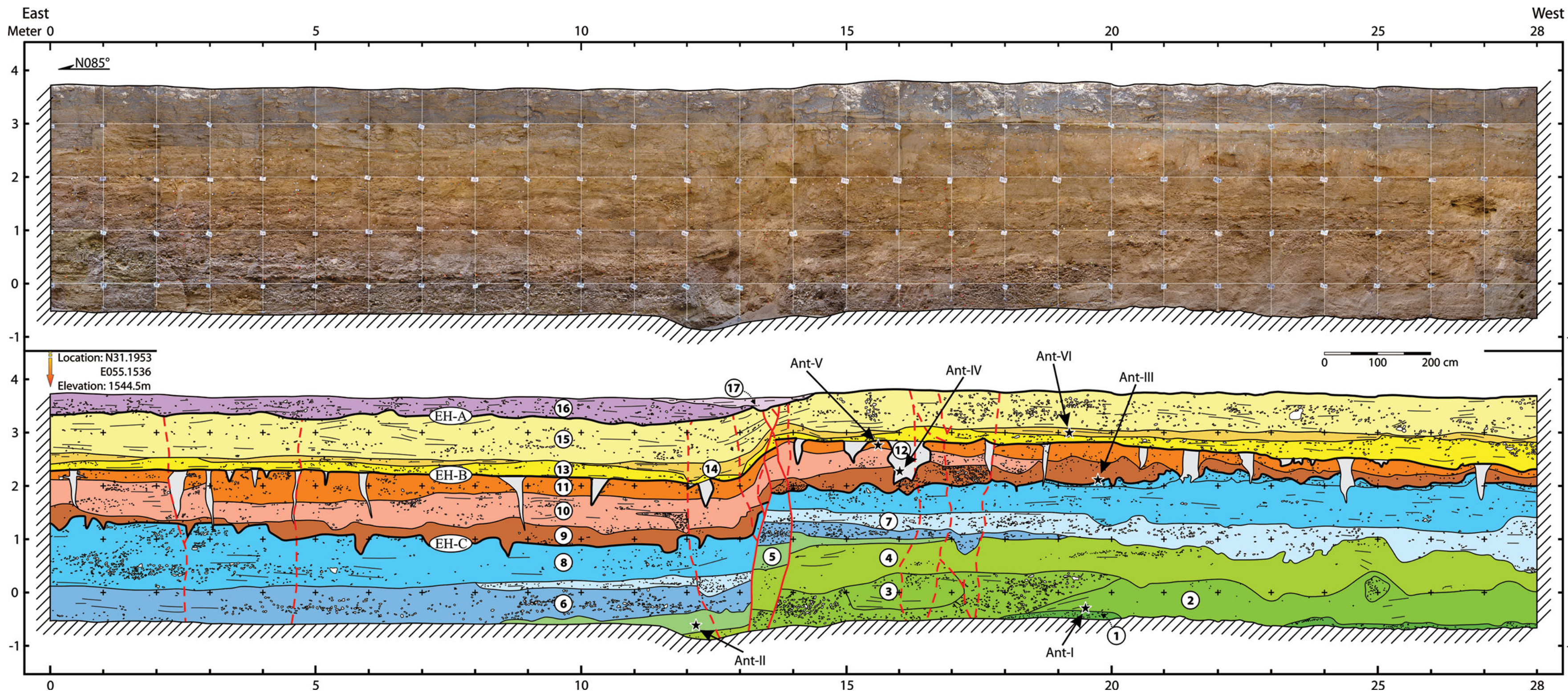

Figure 5. Top panel: photomosaic of southern trench wall (see Fig. 3 for location). Bottom panel: corresponding log, with labels marking the stratigraphic units. Faults and fractures are shown with red and dashed red lines, respectively. Short black lines represent bedding of sedimentary layers. Event horizons discussed in text are labelled as EH-A, EH-B and EH-C. Labelled black stars locate the OSL samples. Sample Ant-I, collected west of the fault zone at 4.1-m deep within unit 2, yields an age of 13.6 ± 1.3 ka. Sample Ant-II, collected east of the fault zone at 4.2-m deep within unit 5, yields an age of 12.4 ± 0.6 ka. Sample Ant-III, collected at 1.5-m deep in a sandy lens of unit 9, yields a poorly constrain ages between 11.5 and 3.3 ka. Sample Ant-IV, collected at 1.5-m deep at the base of a fissure filled with eolian and run-off sand deposits within unit 12, yields an age of 6.2 ± 0.6 ka. Sample Ant-V, collected at 1-m deep within unit 11, yields an age of 7.1 ± 0.7 ka. Sample Ant-VI, collected at 0.8-m deep in a sandy lens within unit 14, yields an age of 6.2 ± 0.4 ka.

Table 1. Detailed description of the units observed in the trench excavated across the Anar fault, corresponding stratigraphic column and log are shown in Figs 4 and 5, respectively.

Unit	Detailed stratigraphic explanation
17	Light grey to cream, poorly stratified, silty sand with some angular gravels (20 per cent, 0.5–2 cm).
16	Light cream, fairly stratified, medium consolidated, angular gravels (60 per cent, 0.5–6 cm), with sand and silt matrix and some gypsiferous cementation.
15	Buff to light grey, well stratified, medium consolidated, angular gravels (50 per cent, 0.5–10 cm), with sand and silt matrix and some gypsiferous cementation.
14	Grey to buff grey, thinly stratified, medium consolidated sand and angular granules (0.5–4 cm) with cross-bedding.
13	Grey, well stratified, medium to well consolidated, coarse sand with angular granules and few pebbles (30 per cent, 0.2–6 cm). The unit bottom is erosive and rests both on units 12 and 11.
12	Light cream to grey, sandy fissure fills and sand-blows.
11	Brown to olive cream, roughly stratified, medium to well consolidated, silts and sands with some channels of angular gravels (40 per cent, 0.1–4 cm). The top exhibits a hard gypsiferous calcrete.
10	Cream to grey, fairly stratified, poorly consolidated, coarse sands and angular gravels (50 per cent, 0.1–3 cm) with sandy–silty matrix and some cross-bedding.
9	Reddish brown to brownish grey, non-stratified, semi-consolidated coarse sand, with clayish silt matrix, including some channels of angular gravels (90 per cent, 2–15 cm) with silt matrix.
8	Cream to brownish grey, fairly stratified, well consolidated, angular granules and pebbles (60 per cent, 0.2–3 cm), with silty sand matrix, including some small cobbles and traces of sulphate calcrete within the coarser levels.
7	Grey to brownish grey, poorly stratified, poorly sorted angular pebbles (70 per cent, 0.5–10 cm), with sandy silt matrix.
6	Cream to brown, fairly stratified, angular granules and pebbles (80 per cent, 0.2–4 cm), with silty sand matrix, including some sparse big cobbles and silty sand lenses.
5	Buff to light grey, fairly stratified, loose silt and sand.
4	Grey to light grey, poorly stratified, well sorted, silty sands with some cross-bedding and gravel lenses.
3	Grey, fairly stratified, well consolidated, medium to well sorted, coarse angular gravels (90 per cent, 0.5–10 cm) with silty sand matrix, including some sparse bigger cobbles and clayish silty sand lenses.
2	Grey, stratified, loose, silty sand, with some cross-bedding.
1	Grey, poorly stratified, well consolidated, angular pebbles (>20 per cent, 0.5–3 cm) with silty sand matrix.

tubes (Fig. 5). The Single Aliquot Regeneration (SAR) protocol (e.g. Murray & Wintle 2000) was employed for the equivalent dose (De) measurement once quartz had been extracted and cleaned from each sample. The analytical procedures employed are identical to that applied to similar samples from the neighbouring Sabzevar, Doruneh and Dehshir faults (Fattahi *et al.* 2006, 2007, 2010; Le Dortz *et al.* 2011). To make all data consistent, three samples with ages that were previously published in Le Dortz *et al.* (2009), including one sample collected approximately 8 km farther north (OSL-2 on Fig. 1 and in Table 2), have been refined in the light of procedural development outlined by Fattahi *et al.* (2010). Table 2 provides the relevant information for OSL ages in years from present (2010) with 1σ errors.

Initial attempts to use single grains for De determination failed due to the dimness of OSL signal. As a result, De measurements were undertaken on 9.6-mm diameter aliquots containing approximately 1500–2000 grains. Although normally this might result in averaging out of any multiple dose component within a sample, here it is assumed that for these dim samples the luminescence signal from each aliquot was produced by a relatively few number of bright grains and thus may be considered as almost measuring at single grain level. Therefore, the De distribution of the single aliquot De measurements is considered to be almost a true reflection of the actual De distribution within a sample. For samples showing unimodal, apparently normally distributed De's with a low overdispersion (Ant-I and Ant-IV in Table 2), which are interpreted as having had the OSL signal reset (bleached) before burial, central age model (CAM) was employed for calculation purposes. For the remaining samples (Ant-II, Ant-III, Ant-V, Ant-VI and OSL-2 in Table 2), the depositional setting, field sedimentary logs and the scatter of the replicate aliquot De data indicated that before burial, full resetting (bleaching) of the OSL signal had not taken place and/or that the sediments had undergone some post-depositional disturbance (Bateman *et al.* 2007). Indeed, the small size of the catchment area at the trench site, less than 20 km^2, is indicative of a rapid transport before the emplacement of the fan (Le Dortz *et al.* 2009). The great majority of the Anar trench deposits come from high-discharge depositional events with limited surface exposure, which favour partial bleaching (Rittenour 2008). As a consequence, finite mixture model (FMM; Roberts *et al.* 2000) was used where samples showed skewed, scattered or multimodal distributions and the dominant De component was used for age calculations (as in Fattahi *et al.* 2010). This approach yielded ages in accordance with site stratigraphy except for sample Ant-III whose age was too young. This sample has exhibited the highest overdispersion value (51 per cent, Table 2) of all measured samples and three De component were extracted by FMM for this sample, the highest representing 30 per cent of the signal and the smallest 47 per cent. It is possible to get an age that fits with stratigraphy using the higher two De components extracted using FMM, corresponding to ages of 7.3 ± 0.5 and 10.7 ± 0.8 ka, respectively. However, there are no good reasons to accept components representing only 23 or 30 per cent of the data over the 47 per cent of the data incorporated into the dominant smallest FMM component. The latter cannot be ignored on the basis of partial bleaching as it has a lower De and is unlikely to represent post-depositional disturbance, as it is the dominant De component but also based on observed bedding within the unit. However, unlike most other samples studied, Ant-III was sampled actually on a stratigraphic boundary (between units 8 and 9). As the dose-rate for this sample is based only on the activity from unit 9, a difference in the gamma radiation dose received from unit 8 might help explain the apparent underestimation of age based on the lowest FFM De

Table 2. Calculated OSL ages on the Anar samples with their parameters. Ages have been calculated for quartz grains with size ranging between 90 and 150 μm.

Sample	Latitude °N	Longitude °E	Depth (m)	Water (per cent)	K (per cent)	U (per cent)	Th (per cent)	Annual dose rate (Gy ka^{-1})	overdispersion (per cent)	Skewness	CAM De (Gy)	FMM De (Gy)	Age (ka)
Ant-I (OSL1-b)[a]	31.1952	55.1534	4.1	2	0.93 ± 0.03	1.16 ± 0.05	4.0 ± 0.1	1.64 ± 0.05	24	0.69	22.3 ± 1.90		13.6 ± 1.3[b]
Ant-II	31.1952	55.1534	4.2	0.4	0.77 ± 0.03	0.97 ± 0.05	3.4 ± 0.1	1.42 ± 0.04	27	4.09	16.1 ± 0.90	17.5 ± 0.47	12.4 ± 0.6[c]
Ant-III	31.1952	55.1534	1.7	1.1	0.97 ± 0.01	1.23 ± 0.05	4.3 ± 0.1	1.75 ± 0.04	51	2.1	9.7 ± 1.09	6.1 ± 0.24	3.5 ± 0.2[c]
Ant-IV	31.1952	55.1534	1.5	0.6	0.94 ± 0.01	1.44 ± 0.05	3.7 ± 0.1	1.78 ± 0.14	20	0.01	11.0 ± 0.61		6.2 ± 0.6[b]
Ant-V	31.1952	55.1534	1.0	0.3	0.99 ± 0.01	1.72 ± 0.05	4.2 ± 0.1	1.96 ± 0.14	25	0.35	13.5 ± 0.90	13.9 ± 0.70	7.1 ± 0.7[c]
Ant-VI (OSL1-a)[a]	31.1952	55.1534	0.8	0.6	1.21 ± 0.01	1.60 ± 0.05	5.9 ± 0.1	2.20 ± 0.05	42	0.94	11.6 ± 1.39	13.7 ± 0.56	6.2 ± 0.4[d]
OSL-2	31.2697	55.1337	0.8	1.1	1.06 ± 0.01	1.33 ± 0.05	4.0 ± 0.1	1.90 ± 0.05	41	2.39	20.1 ± 2.16	19.3 ± 0.76	10.1 ± 0.6[d]

[a]Parenthesis contains the sample label used by Le Dortz *et al.* (2009).
[b]Age based on De determined using central age model (CAM; Galbraith *et al.* 1999).
[c]Age based on De determined using the dominant component of finite mixture modelling (FMM; Roberts *et al.* 2000).
[d]Age previously published, now refined using finite mixture modelling (FMM; Roberts *et al.* 2000).

component. Unfortunately, field-based gamma-spectrometer readings or material for analysing the radioactive elements within unit 8 were not available to test this and so the age of Ant-III has not been included within the subsequent site interpretation. Thus, the ages of the trench units have been constrained based on only five OSL ages (Ant-I, Ant-II, Ant-IV, Ant-V and Ant-VI).

AGES OF TRENCH UNITS

The samples collected within the trench define a time range spanning from 5.8 to 14.9 ka. The oldest age Ant-I (13.6 ± 1.3 ka) stands at the bottom of the trench and belongs to one of the oldest stratigraphic units (unit 2), it indicates that all the trench units should be younger than 15 ka. As the youngest OSL sample Ant-VI (6.2 ± 0.4 ka) is located at 0.8 m below the surface (unit 14), these ages define a maximum time interval between 0 and 14.9 ka and a minimum one between 6.6 and 12.3 ka, indicating that the trench deposits aggraded during the uppermost Marine Isotopic Stage 2 (MIS-2 ≈ 12–22 ka) and part or the entirety of MIS-1. The age of the fan surface at the trench site appears poorly constrained between 0 and 6.6 ka.

A proxy to the surface age may be obtained by estimating average sedimentation rates. Assuming this fan surface is still active, the whole 5.9 m of sedimentary units seen in the trench should have been aggraded during the last 14.9 or 12.3 ka at an overall sedimentation rate ranging between 0.4 and 0.48 mm yr^{-1}. Deposit thickness above the samples Ant-I (13.6 ± 1.3 ka) and Ant-II (12.4 ± 0.6 ka) yield slightly lower rates ranging between 0.28 and 0.36 mm yr^{-1}. Conversely, if one assumes the top of the fan surface was abandoned just after 6.6 ka, the oldest possibility for the youngest sample (Ant-VI), the sedimentation rate may have reached 1 mm yr^{-1}. These two extreme hypotheses raise the problem of the abandonment age of the alluvial fan at the precise location where the trench was excavated. The refined age of OSL-2 (10.1 ± 0.6 ka versus 11.8 ± 6.5 ka in Le Dortz *et al.* 2009), which is sampled some 8 km north of the trench (see location on Fig. 1, see also figs 4a and 7 in Le Dortz *et al.* 2009) at 0.8 m below the surface of another fan on the riser of a ≈4.5-m incised dry stream, suggests that its surface was abandoned some 9–10 ka ago at this site whereas the fan surface at the trench site cannot be older than 6.6 ka. These ages are in agreement with the late Pleistocene and Holocene regional climate scenario, for the central and eastern Iran, as recently proposed by Walker & Fattahi (2011). In fact, the satellite image in the vicinity of the trench site (Fig. 3a) shows this location corresponds to an area where the fan surface has been exceptionally preserved from the backward erosion of deeply incised dry streams. Therefore, the late aggradation on the fan surface at the trench site (∼1544 m asl), resulting from surface run-off, lasted until more recently than some 8 km farther north on a more proximal alluvial fan (∼1748 m asl) where Le Dortz *et al.* (2009) collected the sample OSL-2. In conclusion, the best estimate for the aggradation rate of the trench sediments is provided by the depth difference of 3.3 m between Ant-I (13.6 ± 1.3 ka) and Ant-VI (6.2 ± 0.4 ka) samples, this rate ranges between 0.36 and 0.58 mm yr^{-1}. Interestingly, this rate is comparable to the late Pleistocene–Holocene aggradation rates derived from alluvial sediments in similar deposition settings at southwestern Nebraska, Negev desert and Central Iran plateau (Daniels *et al.* 2003; Guralnik *et al.* 2011; Schmidt *et al.* 2011). Consequently, the best averaged net sedimentation rate, if meaningful in such environment, amounts to 0.47 ± 0.11 mm yr^{-1} suggesting that the final aggradation of the trench units ended between 3.6 and 5.2 ka to the west of the fault zone and approximately 1000 yr later to the east of the fault zone accounting for the thickness of units 16 and 17. The abandonment age of the fan surface at the trench site (4.4 ± 0.8 ka) is comparable with late Holocene drought cycles at 4.2 ka, proposed by Staubwasser *et al.* (2003) to the southeast of the Persian Gulf.

SEISMIC EVENT IDENTIFICATION

The surface geomorphology, particularly, the characteristics of the fault scarp, detailed geological and structural analyses of the trench walls (bed unconformities, sealed fault strands and fissure fills or sand-blows) and restoration of the trench log permit to trace three individual event horizons that correlate with three destructive past earthquakes, which ruptured the ground surface. The evidence for these three seismic events, which are labelled A, B and C from the youngest to the oldest, is presented below.

'Event A', the youngest event is responsible for the 35-cm-high, E-facing scarp, which is observed at the surface in the vicinity of the trench (Figs 3b and c). The trench log shows this scarp is located above a nearly 1-m wide, steep faulted zone associated with an E-facing flexure of the upper trench units; that is, downthrown to the east (Fig. 5). Units 16 and 17 are neither observed west of the fault zone nor warped eastward. They rest unconformably on unit 15 dipping about 25°E (Fig. 6), hence indicating the faulting and flexuring deformation post-date unit 15 and pre-date units 16 and 17. As there are no significant thickness differences of the upper trench units on both sides of the fault zone, the faulting and flexuring deformation appear to result from a sudden and discrete slipping event on the fault zone instead of a continuous shear; that is, creep slip (Fig. 7, step 1). In as much as the upper trench units are seen faulted up to unit 15, the discrete slipping event should relate to an earthquake that ruptured the surface producing the scarp. The event horizon of this earthquake locates on the top boundary of unit 15, so that it stands between this latter and units 16 and 17 to the east of the fault and corresponds approximately with the present-day topographic surface to the west of the fault. This suggests that the

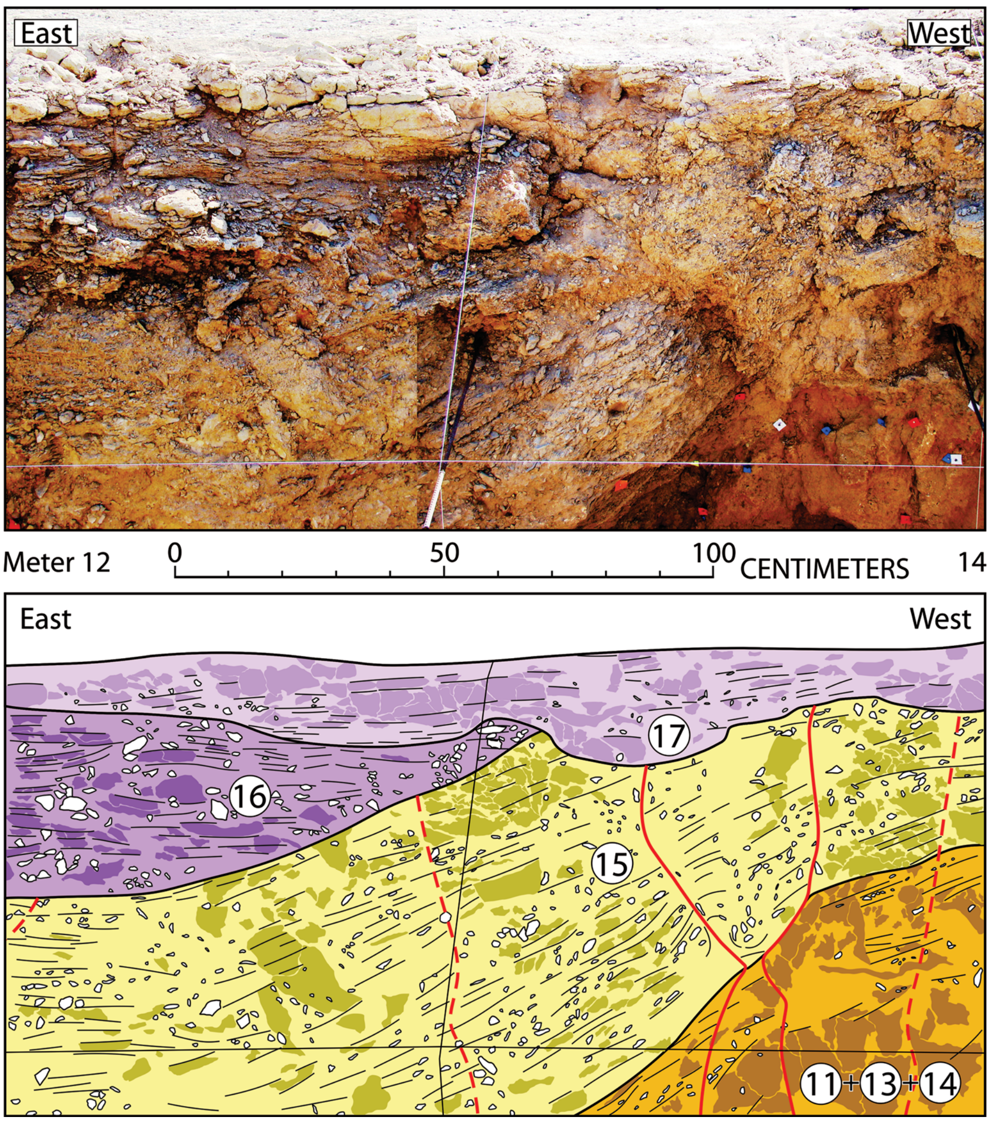

Figure 6. Photomosaic (top) and interpretation (bottom) of the main faulted zone showing evidence for the most recent earthquake (event A). Units 11–15, affected by faulting, are warped downward, while undeformed units 16 and 17 lie unconformably atop. Faults and tiny fractures are shown as red and dashed red lines, respectively.

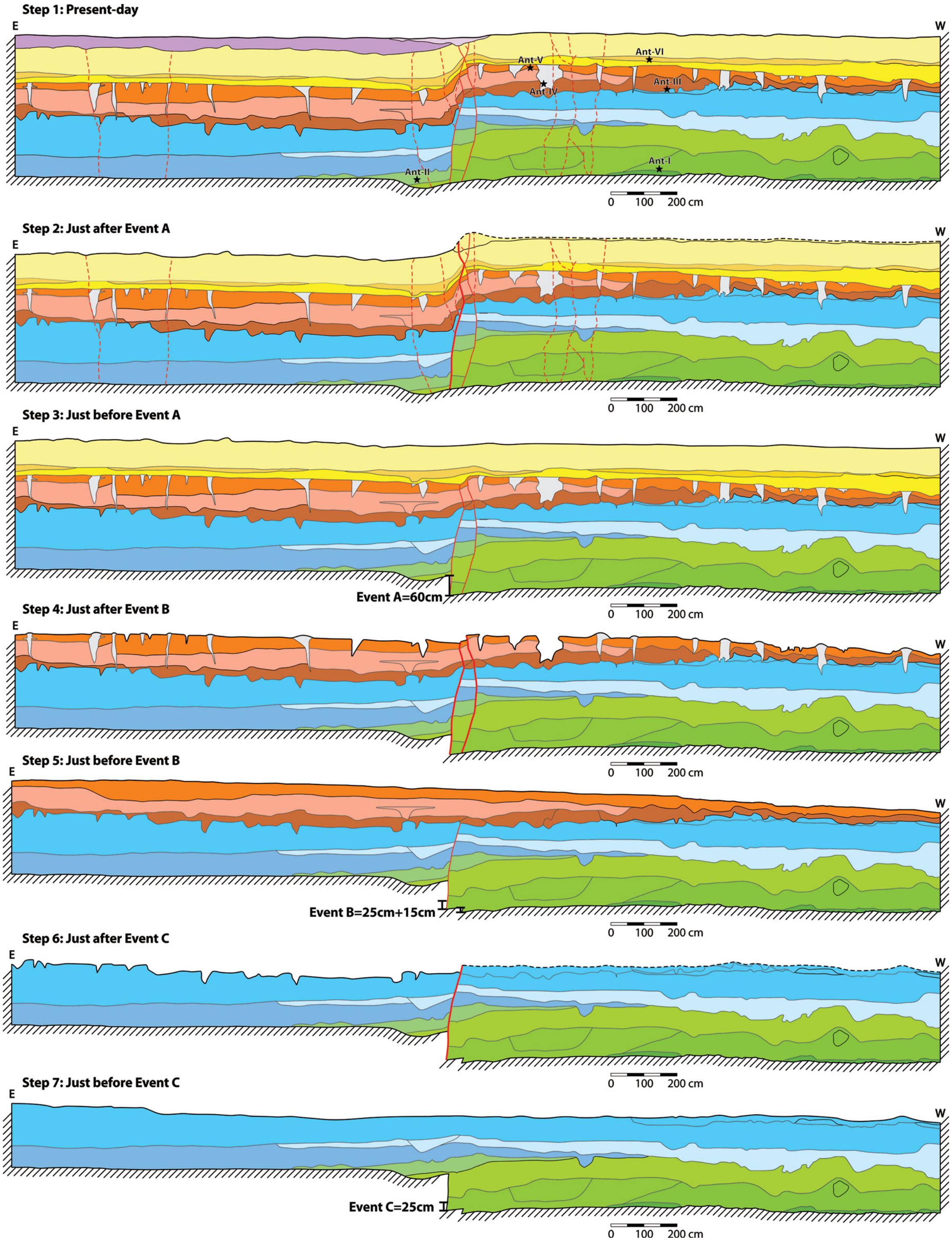

Figure 7. Schematic view of possible restoration of trench log showing sequence of faulting and depositional phases from present-day (step 1) to before the oldest palaeoearthquake (step 7). The trench log has been simplified for clarity. Dashed black lines show inferred ground surface before the erosion. Step (1) is present-day situation. Step (2) is E-facing fault scarp formed during the most recent earthquake. Step (3) is restoration of the ground surface to its position before event A showing a vertical displacement of about 60 cm created by faulting on the eastern branch. Step (4) is the penultimate earthquake denoted by open fissures and cracks formed near the main faulted zone. Sand-blows also emplaced in both sides and away of the main faulted zone. Step (5) is restoration of the ground surface to its position before event B showing vertical displacement created during penultimate earthquake on the eastern and western fault branches about 25 and 15 cm, respectively. Step (6) is the oldest earthquake, it has produced some surficial fissures within downthrown (eastern) block and a 25-cm-high E-facing fault scarp. Step (7) is restoration of the ground surface to its position before event C, showing a vertical displacement of about 25 cm.

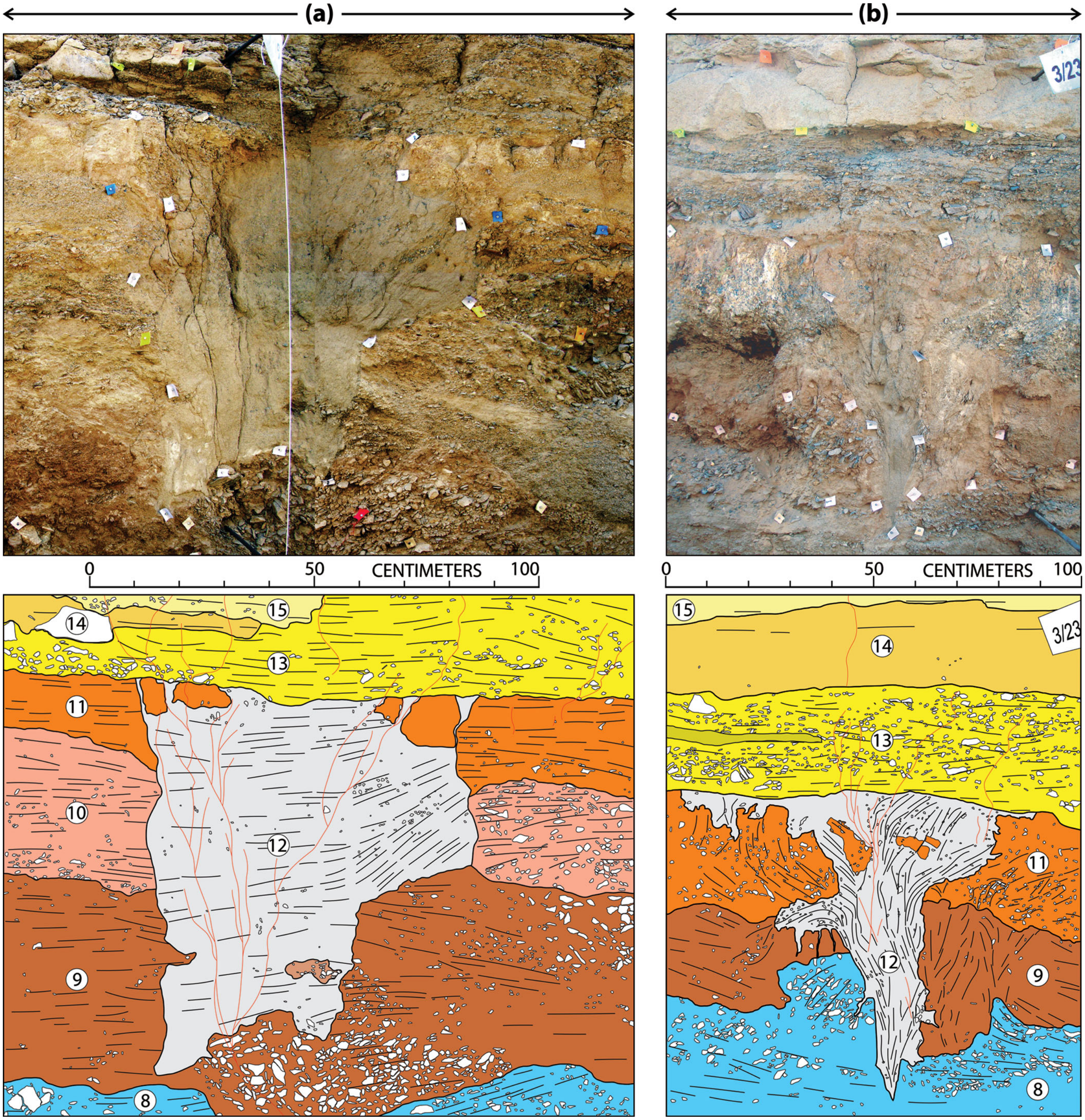

Figure 8. Evidence for the penultimate earthquake (event B) encountered in a fissure fill and a liquefaction feature (sand-blow) at 16 and 22 m of the trench log, respectively. Red lines correspond to tiny cracks post-dating the penultimate earthquake. (a) Photomosaic of fissure filled with eolian sands and silts and interpretative sketch. The fissure is ~85-cm deep and up to ~55-cm wide, tapering downward through unit 9. Colours denote stratigraphy as shown in Figs 4 and 5. The material at the base of the fissure includes a collapsed piece from sidewall and grades into interbedded sand and silt layers. The fissure is sealed by a grey, well-stratified, surficial run-off deposit (unit 13). (b) Photomosaic and interpretative sketch of a sand-blow (unit 12) made of sandy material of unit 8 injected into and deforming units 9 and 11. Hydraulic fractures, vertical and oblique alignments of dragged sands and gravels deform the host sediments close to the liquefaction pillar.

western block has been slightly eroded and partly concealed by units 16 and 17 so that its present-day height underestimates its original height at the time of the earthquake (Fig. 7, step 2). Then, unit 17 is a local sag pond deposit caused by event A.

Backstripping of event A suggests its vertical throw is of some 60 cm (Fig. 7, step 3), confirming that the 35-cm-high scarp at the surface has been partly degraded. Taking into account the Anar fault is dominantly a strike-slip fault (Fig. 2), the 60 cm of vertical displacement should be associated with at least a couple of metres of right-lateral displacement. Then, the magnitude of event A should be at least on the order of $M_w \approx 7$. The age of event A is poorly constrained as the uppermost OSL sample (Ant-VI), which is at

0.8-m depth, comes from unit 14. This indicates only that event A is younger than 6.6 ka. Tentatively, the sediment thickness, which stands between the sample Ant-VI and the event horizon of event A, may be used to propose a rough estimate of the youngest possible age for this seismic event based on the aggradation rate between Ant-VI and Ant-I. Since aggradation of unit 15 ended between 3600 and 5200 yr (see previous section), event A should not be younger than 3600 yr and might be as old as 5200 yr. This time interval will be considered as the preferred age of event A in the following discussion.

'Event B', the penultimate event, is easily determined from analysis of the trench walls. Several filled fissures (unit 12), which post-date unit 11 and pre-date unit 13, are seen (Figs 5 and 7, step 4). A careful analysis of these filled fissures permits to conclude they correspond indeed to either open cracks or sand-blows (Figs 8a and b). It is possible to observe that these features formed suddenly as they disrupt the hard gypsiferous calcrete (e.g. Fig. 8b), which is located in the top part of unit 11. Thus, the interface between units 11 and 13 corresponds to the event horizon of event B. The backstripping analysis of the trench log (Fig. 7), removing the effects of event A and the units aggraded between events A and B, allow reconstructing the event B horizon just after the penultimate earthquake (Fig. 7, step 4). This reconstruction suggests that the rupture of event B should have occurred on two parallel fault strands of the Anar fault zone, totalling a vertical throw of some 40 cm, distributed into 25 cm on the eastern strand and 15 cm on the western one. Thus, the penultimate earthquake appears to have a vertical throw close to that of the last one, hence a magnitude lightly comparable with the one of event A. The age of event B is well constrained by three OSL ages (Ant-V, Ant-IV and Ant-VI) and bracketed between 5.8 and 7.8 ka yielding an average age of 6.8 ± 1 ka for this earthquake (Fig. 9).

'Event C', the oldest seismic event, can be safely identified on the trench walls. Evidence for a third earthquake rests on the facts that lower trench units (5–8) exhibit higher vertical throws than middle ones (9–11). Different reconstructions have been tested to restore the trench lower units; the best fit is obtained when considering the interface between units 8 and 9 as the event horizon of a surface-rupturing earthquake (Fig. 7, step 6). This reconstruction favours that event C ruptured along the eastern fault strand with a vertical displacement of about 25 cm. Nevertheless, this vertical displacement is poorly constrained and higher estimates might be obtained according to the amount of erosion chosen (dashed line on Fig. 7, step 6). Even if this vertical throw is poorly determined and appears smaller than the ones of the subsequent earthquakes, this does not imply a much smaller magnitude as the amount of coseismic vertical displacement is highly variable along a strike-slip fault (e.g. Barka 1996; Barka *et al.* 2002). The age of event C is not well constrained; it occurred before the OSL age of sample Ant-V (7.1 ± 0.7 ka) and after that of Ant-II (12.4 ± 0.6 ka) so that it is bracketed within the interval between 6.4 and 13 ka, with a minimum interval of 4 ka (Fig. 9). We have investigated the possibility for a fourth event in the lowermost part of the trench (Fig. 5). However, the lowermost units (1–4) cannot be followed on the eastern side of the trench precluding the possibility to document an additional event.

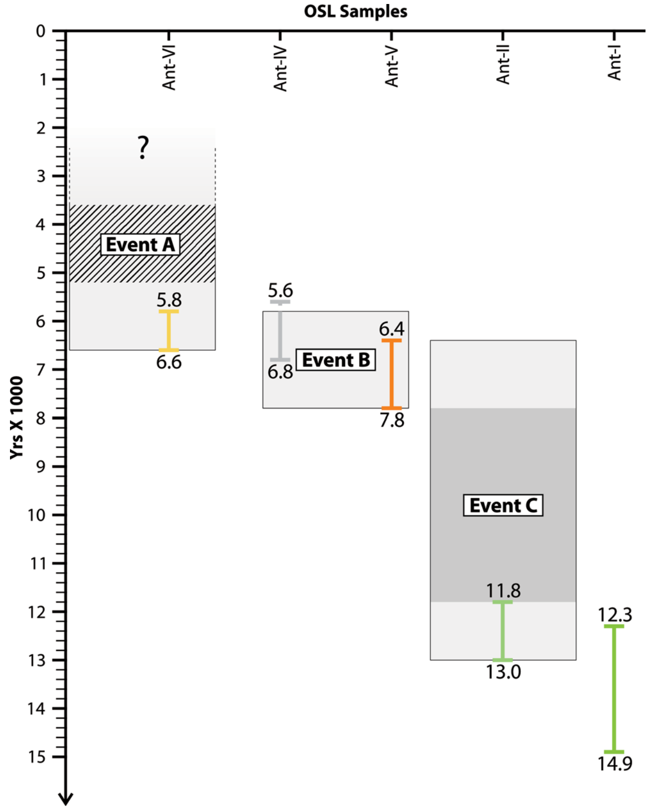

Figure 9. Five well-constrained OSL ages place bounds on the ages of the three palaeoearthquakes (A, B and C) identified in the Anar trench exposure. Light grey areas represent the maximum time windows for the past earthquakes, dark grey pointing the minimum time window for event C. For event A, hatched domain shows the preferred time interval of the earthquake (4.4 ± 0.8 ka). Colour codes are similar to units shown in Figs 4 and 5. Question mark illustrates the ambiguity due to the lack of ages in units post-dating the most recent earthquake (16 and 17).

DISCUSSION AND CONCLUSIONS

Due to the reduced size of the surface sag pond, a 3-D trench exploration was not undertaken at the trench site so that the slip per event was not directly measurable for the three identified seismic events, A, B and C. Accounting for the lack of morphological segmentation along the Anar fault (Le Dortz *et al.* 2009) and the excavation of a single trench, there are no possibilities to calculate confidently any magnitude. The restored vertical throws per event suggest only that the related magnitudes are more likely on the order of $M_w \approx 7$ (see previous section). The right-lateral offsets observed at the surface (Figs 2 and 3a) permit to reinforce this inference. Deeply incised intermittent streams are seen offset by 8 ± 0.5 m (Le Dortz *et al.* 2009 and Fig. 3a) whereas several weakly incised small dry gullies show offsets of 3 ± 0.5 m only (Fig. 2). Considering these lower offsets were more likely formed during the most recent earthquake, they provide the best estimate for the coseismic horizontal slip of event A. Such a coseismic slip at the surface agrees with a magnitude close to 7. Thus the higher offsets, which are only observed where the alluvial surface is older, should represent the cumulative horizontal slip of the last three events that are seen in the trench. Therefore, the three events, which are observed within the trench to the north of Anar city, should have had slip per event on the order of 3 m, suggesting they are of similar magnitudes.

Overall, the new data presented in this paper give evidence for at least three seismic events of similar sizes on the Anar fault (Fig. 9). OSL age of Ant-I sample indicates that the aggradation of the trench units did not started much before 14.9 ka or to the latest by 12.3 ka. Because only three events have occurred during the last 15 ka, this provides a rough estimate of at most 5 ka for the average maximum time interval between two earthquakes. The youngest age possibility may reduce this average time interval between two earthquakes to ≈4 ka. Considering the best estimates of average ages for the three seismic events A, B and C are: 4.4 ± 0.8, 6.8 ± 1 and 9.7 ± 3.3 ka, respectively (Fig. 9), the time interval between two subsequent earthquakes is ill defined and might vary significantly. Nevertheless, the average ages for events A, B and C indicate that the intervals between two subsequent earthquakes should be 2400 and 2900 yr between events A–B and B–C, respectively. As the elapsed time since the last earthquake is 3600 yr at least and 5200 yr at most, this suggests we are getting close to the end of the seismic cycle and may anticipate a destructive earthquake for the Anar city in the near future.

Finally, the cumulative offset of 8 ± 0.5 m (Le Dortz *et al.* 2009) post-dating fan aggradation and the refined age of fan abandonment given by OSL-2 sample (10.1 ± 0.6 ka) confirm a minimum slip rate estimate of 0.8 ± 0.1 mm yr^{-1} for the Anar fault. Then, the westernmost prominent right-lateral faults of the Central Iran plateau, namely the Dehshir and Anar faults, which are active though void of historical and instrumental earthquakes, are characterized by slip rates close to 1 mm yr^{-1} (Le Dortz *et al.* 2009, 2011). Such faults have repeatedly produced destructive earthquakes with large magnitudes ($M_w \approx 7$) and long recurrence interval of several thousands of years during the Holocene (Nazari *et al.* 2009; Fattahi *et al.* 2010 and this paper). This demonstrates that the Central Iran plateau does not behave totally as a rigid block and that its moderate internal deformation is nonetheless responsible for a significant seismic hazard.

ACKNOWLEDGMENTS

This study benefited of the logistic and financial assistance from Geological Survey of Iran. Université Pierre et Marie Curie and INSU-CNRS provided complementary funding for the fieldwork and OSL measurements. M. Foroutan acknowledges a grant from the French Embassy in Tehran for part of his PhD thesis and complementary support from UPMC-ISTeP. David Lambert, Attaché Scientifique et Culturel, is thanked for his continuing support to the cooperation between UPMC and GSI. M. Hosseini from Kerman GSI office helped with the logistics of the fieldwork. B. Oveisi, M. Nazem Zadeh, A. Agha Hosseini and M.A. Shokri are thanked for various contributions to the fieldwork, H. Bani Assadi and M. Adhami for their safe driving in the field. M. Fattahi would like to thank the research department of the Tehran University. We thank two anonymous reviewers for helpful and constructive comments.

REFERENCES

Ambraseys, N.N. & Jackson, J.A, 1998. Faulting associated with historical and recent earthquakes in the Eastern Mediterranean region, *Geophys. J. Int.,* **133,** 390–406.

Ambraseys, N. & Melville, C., 1982. *A History of Persian Earthquakes,* Cambridge University Press, Cambridge.

Barka, A.A., 1996. Slip distribution along the North Anatolian Fault associated with the large earthquakes of the period 1939 to 1967, *Bull. seism. Soc. Am.,* **86**(5), 1238–1254.

Barka, A.A. *et al*., 2002. The surface rupture and slip distribution of the 17 August 1999 Izmit Earthquake (M 7.4), North Anatolian Fault, *Bull. seism. Soc. Am.,* **92,** 43–60.

Bateman, M.D., Boulter, C.H., Carr, A.S., Frederick, C.D., Peter, D. & Wilder, M., 2007. Preserving the palaeoenvironmental record in drylands: bioturbation and its significance for luminescence derived chronologies, *Sediment. Geol.,* **195**(1–2), 5–19.

Daniels, J.M., 2003. Floodplain aggradation and pedogenesis in a semiarid environment, *Geomorphology,* **56,** 225–242.

Fattahi, M., Walker, R., Hollingsworth, J., Bahroudi, A., Nazari, H., Talebian, M., Armitage, S. & Stokes, S., 2006. Holocene slip-rate on the Sabzevar thrust fault, NE Iran, determined using optically-stimulated luminescence (OSL), *Earth planet. Sci. Lett.,* **245,** 673–684.

Fattahi, M., Walker, R.T., Khatib, M.M., Dolati, A. & Bahroudi, A., 2007. Slip-rate estimate and past earthquakes on the Doruneh fault, eastern Iran, *Geophys. J. Int.,* **168,** 691–709.

Fattahi, M. *et al*., 2010. Refining the OSL age of the last earthquake on the Dheshir fault, Central Iran. *Quat. Geochronol.,* **5,** 286–292, doi:10.1016/j.quageo.2009.04.005.

Galbraith, R.F., Roberts, R.G., Laslett, G.M., Yoshida, H. & Olley, J.M., 1999. Optical dating of single and multiple grains of quartz from Jinmium rock shelter, northern Australia, part 1, Experimental design and statistical models, *Archaeometry,* **41,** 339–364.

Guralnik, B., Matmon, A., Avni, Y., Porat, N. & Fink, D., 2011. Constraining the evolution of river terraces with integrated OSL and cosmogenic nuclide data, *Quat. Geochronol.,* **6,** 22–32.

Jackson, J. & D. McKenzie, 1984. Active tectonics of the Alpine-Himalayan Belt between western Turkey and Pakistan, *Geophys. J.R. astr. Soc.,* **77,** 185–264.

Le Dortz, K. *et al*., 2009. Holocene right-slip rate determined by cosmogenic and OSL dating on the Anar fault, Central Iran, *Geophys. J. Int.,* **179,** 700–710.

Le Dortz, K. *et al*., 2011. Dating inset terraces and offset fans along the Dehshir fault combining cosmogenic and OSL methods, *Geophys. J. Int.,* **185,** 1147–1174.

Meyer, B. & Le Dortz, K., 2007. Strike-slip kinematics in Central and Eastern Iran: estimating fault slip-rates averaged over the Holocene, *Tectonics,* **26,** TC5009, doi:10.1029/2006TC002073.

Meyer, B., Mouthereau, F., Lacombe, O. & Agard, P., 2006. Evidence of quaternary activity along the Deshir Fault, *Geophys. J. Int.,* **164,** 192–201.

Murray, A.S. & Wintle, A.G., 2000. Luminescence dating of quartz using an improved single-aliquot regenerative-dose protocol, *Radiat. Meas.,* **32,** 57–73.

Nazari, H. *et al*., 2009. First evidence for large earthquakes on the Deshir Fault, Central Iran Plateau, *Terra Nova,* **21,** 417–426.

Rittenour, T.M., 2008. Luminescence dating of fluvial deposits: applications to geomorphic, palaeoseismic and archaeological research, *Boreas,* **37,** 613–635.

Roberts, R.G., Galbraith, R.F., Yoshida, H., Laslett, G.M. & Olley, J.M., 2000. Distinguishing dose populations in sediment mixtures: a test of single-grain optical dating procedures using mixtures of laboratory-dosed quartz, *Radiat. Meas.,* **32,** 459–465.

Schmidt, A., Quigley, M., Fattahi, M., Azizi, Gh., Maghsoudi, M. & Fazeli, H., 2011. Holocene settlement shifts and palaeoenvironments on the Central Iranian Plateau: investigating linked systems, *Holocene,* **21**(4), 583–595, doi:10.1177/0959683610385961.

Staubwasser, M., Sirocko, F., Grootes, P.M. & Segl, M., 2003. Climate change at the 4.2 ka BP termination of the Indus valley civilization and Holocene south Asian monsoon variability, *Geophys. Res. Lett.,* **30**(8), 1425, doi:10.1029/2002GL016822.

Vernant, P. *et al*., 2004. Present-day crustal deformation and plate kinematics in the Middle East constrained by GPS measurements in Iran and northern Oman, *Geophys. J. Int.,* **157,** 381–398.

Walker, R. & Fattahi, M., 2011. A framework of Holocene and Late Pleistocene environmental change in eastern Iran inferred from the dating of periods of alluvial fan abandonment, river terracing, and lake deposition, *Quat. Sci. Rev.,* **30,** 1256–1271, doi:10.1016/j.quascirev.2011.03.004.

Walker, R. & Jackson, J., 2004. Active tectonics and late Cenozoic strain distribution in central and eastern Iran, *Tectonics,* **23,** TC5010, doi:10.1029/2003TC001529.